PHYSICAL REVIEW B **76**, 195124 (2007)

Structure and physical properties of type-I clathrate solid-solution $Ba_8Pt_xGe_{46-x-y}\square_y$ ($\square$=vacancy)

N. Melnychenko-Koblyuk, A. Grytsiv, P. Rogl, and M. Rotter
Institute of Physical Chemistry, University of Vienna, A-1090 Wien, Austria

R. Lackner and E. Bauer
Institute of Solid State Physics, Vienna University of Technology, A-1040 Wien, Austria

L. Fornasari and F. Marabelli
Physics Department "Alessandro Volta," University of Pavia, I-27100 Pavia, Italy

G. Giester
Institute of Mineralogy and Crystallography, University of Vienna, Althanstrasse 14, A-1090 Wien, Austria
(Received 18 July 2007; revised manuscript received 19 September 2007; published 28 November 2007)

Formation, crystal chemistry, and physical properties were investigated for the solid-solution $Ba_8Pt_xGe_{46-x-y}\square_y$ ($\square$ is a vacancy) deriving from binary clathrate $Ba_8Ge_{43}\square_3$ with a solubility limit of ~3.5 Pt atoms/f.u. at $T=800$ °C. Structural investigations throughout the homogeneity region confirm isotypism with the cubic primitive clathrate type-I structure (space group type $Pm\bar{3}n$) and lattice parameters ranging from $a=1.0657(2)$ nm for $Ba_8Ge_{43}\square_3$ to $a=1.0752(2)$ nm for $Ba_8Pt_{3.5}Ge_{41.5}\square_{1.0}$. Phase relations for the region concerning the clathrate solution were derived at subsolidus temperatures as well as at 800 °C. Transport properties evidence electrons as the majority charge carriers in the system with a slight dependency on the Pt content. The system is located close to a semiconducting regime with a gap in the electronic density of states of a few thousand K. No low temperature maximum is obvious from thermal conductivity which is dominated by the lattice contribution. Thermal conductivity furthermore documents a high efficiency of phonon scattering on vacancies.

DOI: 10.1103/PhysRevB.76.195124 PACS number(s): 82.75.−z, 61.66.Fn, 72.15.−v, 67.55.Hc

I. INTRODUCTION

Glasslike thermal conductivity besides high electrical conductivity and a high Seebeck coefficient have made clathrates interesting research objects for potential thermoelectric applications. The search for high-performance TE materials in the high-temperature region above 800 K revealed promising results for germanium-based clathrates such as $Ba_8Ga_{16}Ge_{30}$ with a figure of merit close to $ZT=1.35$ at 900 K.[1] Recent research on the physical properties of M =Zn-, Cd-, or Pd-containing clathrate type-I systems $Ba_8M_xGe_{46-x-y}\square_y$ (Refs. 2–4) has demonstrated that increasing Zn, Cd, or Pd content drives the metallic system toward a metal-to-insulator transition. This change in the electronic structure of clathrates can be understood in terms of the Zintl concept where the 4 electrons/f.u. resulting from three framework defects in binary $Ba_8Ge_{43}\square_3$ (formulated as $[Ba^{+2}]_8[Ge^0]_{43}[\square^{-4}]_3)$[5,6] are reduced in a ternary clathrate solution via vacancy filling and/or substitution of four-bonded Ge-framework atoms by elements of lower valency. Compositional adjustment via substitution and doping is therefore a successful route to tune the charge carrier concentration and the electronic density of states at the Fermi level of clathrates for maximum thermoelectric performance in a given temperature range. Only limited information is available on the thermoelectric performance of clathrates stabilized by platinum metals. Formation and crystal structure of type-I clathrates $Ba_8M_xGe_{46-x}$ (M=Pd,Pt, x~6) have been investigated by Cordier and Woll[7] but no link was made to the binary clathrates Ba_6Ge_{25} (Ref. 8) and $Ba_8Ge_{43}\square_3$.[5,6] Therefore the main tasks of the present work are (i) to establish the extension of the single phase clathrate region in the ternary system Ba-Pt-Ge at $T=800$ °C, (ii) to elucidate details of substitution and vacancy concentration in the crystal structure of clathrate type-I, and (iii) to investigate the physical properties for the ternary clathrate type-I solution $Ba_8Pt_xGe_{46-x-y}\square_y$.

II. EXPERIMENT

Alloys with a weight of 1–2 g were prepared by arc melting (weight loss less than 0.1%) on a water-cooled copper hearth in Ti-gettered argon from elemental ingots with minimal purity of 99.9 wt %. The alloys were sealed in evacuated quartz tubes and annealed at 800 °C for 5–7 days before quenching in cold water. Samples with nominal composition $Ba_8Pt_6Ge_{40}$ were annealed at $T=800$, 700, and 500 °C. Details of the various techniques of characterization of composition via light optical microscopy (LOM) and scanning electron microscopy, electron probe microanalysis (EPMA) [binary clathrate Ba_8Ge_{43} and ternary compounds, τ_1 ($BaPtGe_3$) and τ_2 ($BaPt_4Ge_{12}$), were used as standards], of crystal structure [x-ray powder (XRPD) and single crystal diffraction on a single crystal, $Ba_8Pt_{2.65}Ge_{41.68}\square_{1.67}$], and of physical properties (electrical and thermal conductivities and thermopower) have been described in our previous paper on Cd-containing Ge-based clathrates.[2] Spectroscopic ellipsometry measurements have been performed on mechanically

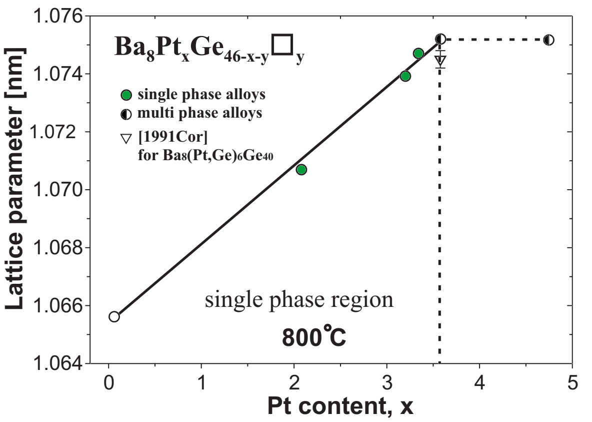

FIG. 1. (Color online) Lattice parameters vs Pt content for $Ba_8Pt_xGe_{46-x-y}\square_y$ alloys. The dashed line denotes the solubility limit of Pt at $T=800$ °C.

polished samples with shining surfaces in a spectral range 1.4– 5 eV, whereas near normal reflectance has been measured from 0.1 to 1.8 eV using a fast Fourier transform spectrometer equipped with a microfocusing accessory.

III. RESULTS AND DISCUSSION

A. Phase equilibria in the Ge-PtGe-$BaGe_2$ region of the Ba-Pt-Ge system

In a first task to elucidate the phase relations in the Ge-rich part of the Ge-PtGe-$BaGe_2$ subsystem at $T=800$ °C, we investigated the ternary clathrate type-I solution extending from binary $Ba_8Ge_{43}\square_3$. Alloys with nominal composition $Ba_8Pt_xGe_{46-x}$ $(0 \leqslant x \leqslant 6)$ ($x=0$, 2, 3, 3.5, and 6) annealed at $T=800$ °C were examined by means of XRPD, LOM, and EPMA. The maximal solubility of 6.58 at. % Pt at $T=800$ °C in $Ba_8M_xGe_{46-x-y}\square_y$ corresponds to about ~3.5 Pt atoms per unit cell and was established by EMPA from a sample with nominal composition $Ba_8Pt_6Ge_{40}$. The alloy was found to be multiphase with a lattice parameter [$a=1.075\,20(2)$ nm] for the clathrate phase. This value is close to that reported by Cordier *et al.*[7] for the clathrate composition given as "$Ba_8(Pt,Ge)_6Ge_{40}$" (Fig. 1). The expansion of the clathrate unit cell with increasing Pt content is in accordance with the atomic size of Pt and Ge (Fig. 1). As the binary clathrate Ba_8Ge_{43} only exists in a small temperature region from $T=770$ °C to $T=810$ °C,[6] the stability range of ternary $Ba_8Pt_xGe_{46-x-y}\square_y$ was tested at lower temperatures. Annealing the sample with nominal composition $Ba_8Pt_6Ge_{40}$ at $T=700$ °C for 10 days or at $T=500$ °C for 150 days in both cases confirmed the clathrate type-I with cell parameters 1.075 00(2) and 1.074 39(2) nm, respectively. Thus we conclude a significant increase of thermodynamic stability for the Pt-based clathrate with respect to binary $Ba_8Ge_{43}\square_3$.

The decrease of the Ba content with increasing Ge/Pt substitution—as revealed by EMPA—is associated with a change in the amount of vacancies in the crystal lattice (see Table I). Assuming a complete Ba sublattice (full occupancy of Ba in 2*a* and 6*c* sites, as proven from x-ray refinements with deviations of less than 1% in occupancy), the vacancy concentration in the framework of the structure could be calculated from EPMA data. Although the amount of vacancies decreases almost linearly with increasing Pt content (Fig. 2), about one vacancy per formula was found at the maximal Pt content of 3.5 at./f.u.

Evaluation of the phase relations at 800 °C (Fig. 3) revealed the existence of two ternary compounds, τ_1 ($BaPtGe_3$) and τ_2 ($BaPt_4Ge_{12}$). τ_1 ($BaPtGe_3$) with $BaNiSn_3$ type ($a=0.4571$, $c=1.0220$ nm, space group $I4mm$) has recently been described by Demchyna *et al.*[9] τ_2 ($BaPt_4Ge_{12}$), observed in this work, is a skutterudite compound with filled $LaFe_4Sb_{12}$ type ($a=0.869\,28$ nm, space group $Im\bar{3}$); it is a skutterudite based on a host lattice entirely built by germanium atoms.[10] It is interesting to note from Fig. 3 that clathrates and skutterudite at 800 °C are separated by a two-phase

TABLE I. Composition and crystallographic data for $Ba_8Pt_xGe_{46-x-y}\square_y$.

Nominal composition	EPMA (at. %)[a] Ba	Pt	Ge	Accepted composition[b,c]	Lattice parameter *a* (nm)	Ge2 in 16*i* (*x*,*x*,*x*)	Ge3 in 24*k* (0,*y*,*z*)
Ba_8Ge_{43}	15.7	0.0	84.3	$Ba_8Ge_{43}\square_3$	1.0657(2)		
$Ba_8Pt_2Ge_{44}$	15.3	3.8	80.8	$Ba_8Pt_{2.0}Ge_{42.3}\square_{1.7}$	1.07069(2)	0.1830(1)	0.1219(2), 0.3163(2)
$Ba_8Pt_3Ge_{43}$	15.3	5.1	79.6	$Ba_8Pt_{2.7}Ge_{41.8}\square_{1.5}$	1.07259(3)	0.18334(8)	0.1207(1), 0.3155(1)
				$Ba_8Pt_{2.7}Ge_{41.7}\square_{1.6}$[d]	1.07344(2)	0.18372(4)	0.12049(8), 0.31365(8)
						[0.18370(3)]	Ge31 [0.1194(1), 0.3105(4)]
							Ge32 [0.1297(8), 0.3409(9)]
$Ba_8Pt_{3.5}Ge_{42.5}$	15.1	6.1	78.8	$Ba_8Pt_{3.3}Ge_{41.6}\square_{1.1}$	1.07470(2)	0.18300(8)	0.1212(1), 0.3135(1)
$Ba_8Pt_6Ge_{40}$	15.1	6.6	78.3	$Ba_8Pt_{3.5}Ge_{41.5}\square_{1.0}$	1.07520(2)	0.1830(3)	0.1218(4), 0.3151(4)

[a] After calibration against system internal standards; standard deviations ≤0.3 at. % Pt.

[b] Ba sublattice (2*a* and 6*c* sites) was found to be complete; structure standardized with program TYPIX (Ref. 12).

[c] Formula from Rietveld refinement.

[d] X-ray single crystal data. $R_{F^2}=\Sigma|F_o^2-F_c^2|/\Sigma|F_o^2|=0.022$. Values in square brackets correspond to refinement with split Ge3 site [0.85(2)Ge31+0.15(2)Ge32].

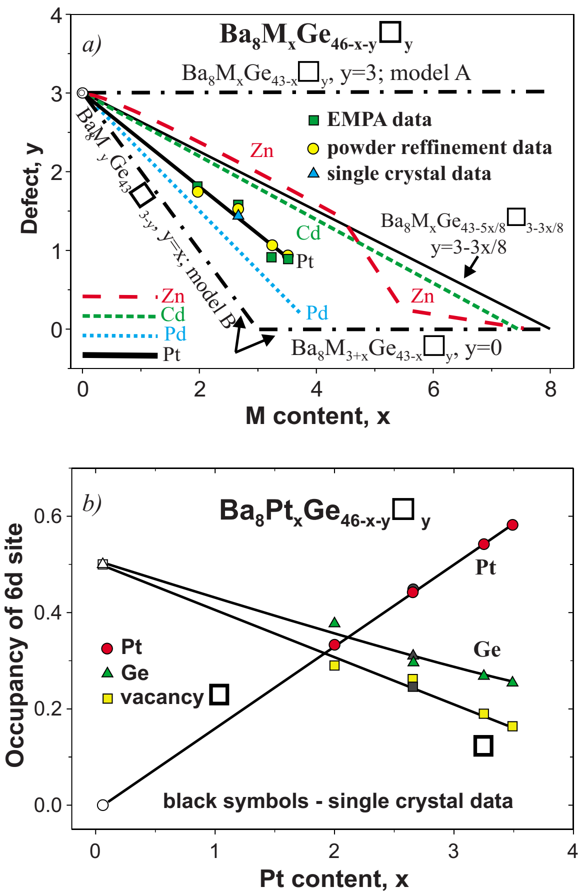

FIG. 2. (Color online) (a) Defect concentration y vs Pt content x; dependences of deficiency from M content ($M=\mathrm{Pt,Pd,Zn,Cd}$) in $Ba_8Pt_xGe_{46-x-y}\square_y$ are compared for two boundary models for the incorporation of M atoms in the lattice of $Ba_8Ge_{43}\square_3$; (b) the 6d site preference for $Ba_8Pt_xGe_{46-x-y}\square_y$.

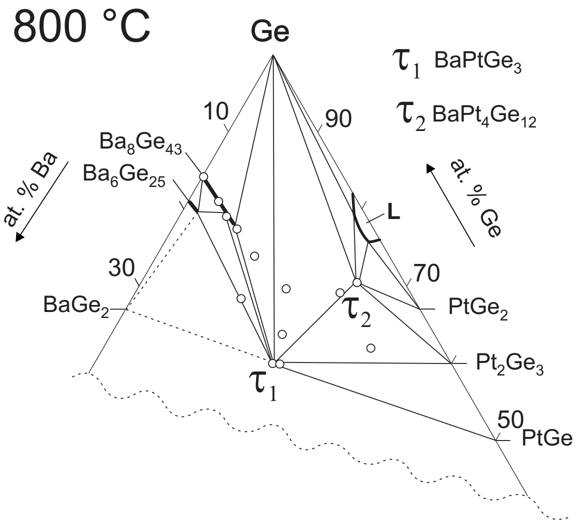

FIG. 3. Partial isothermal section at $T=800\ °C$ for the region Ge-PtGe-$BaGe_2$.

field τ_1+(Ge). The solubility of Pt in clathrate type-IX Ba_6Ge_{25} (Refs. 11 and 13) is limited to less than 2 at. % Pt.

B. Crystal chemistry of $Ba_8Pt_xGe_{46-x-y}\square_y$

As the thermoelectric behavior in intermetallic clathrates is primarily governed by structural parameters such as metal order and vacancy concentration, we attempted to evaluate atom site preferences in $Ba_8Pt_xGe_{46-x-y}\square_y$ from room temperature x-ray powder diffraction data for samples with $0 \leq x \leq 3.5$ assisted by x-ray intensity data from a single crystal, selected from a sample with nominal composition $Ba_8Pt_3Ge_{43}$. Single crystal data were collected at 100, 200, and 300 K. In all cases extinctions were consistent with a primitive cubic lattice (space group $Pm\bar{3}n$, $a\sim 1.1$ nm) and indicated isotypism with the structure of clathrate type I. No extra reflections indicating a larger unit cell $a'=2a$ as reported by Carillo-Cabrera *et al.*[6] were detected in the investigated crystals. The strongly scattering barium atoms were unambiguously located in sites 2a (0,0,0) and 6c $(\frac{1}{4},0,\frac{1}{2})$, while the electron density distribution for the remaining atom sites revealed constant electron densities in both lattice sites 16i and 24k, but an increasing number of electrons in the 6d site with increasing Pt content. In binary Ba_8Ge_{43} (Ref. 6) vacancies are located at the 6d site. As refinement of occupancies for three species in one site (Ge and Pt atoms and vacancies) is not reliable, the Pt content in the 6d site was fixed from EPMA data (carefully calibrated against binary clathrate Ba_8Ge_{43} and PtGe, and ternary τ_1 and τ_2 as standards). Consequently refinement of the Ge content in this site allowed us to determine the number of vacancies (see Table I and Fig. 2). Compositions resulting from refinements of x-ray single crystal and powder diffraction data finally were in fine agreement with overall EPMA data (Table I). The amount of vacancies as a function of M content (M=Pd, Pt, Zn, Cd, see Fig. 2) is compared for two limit models of M atom incorporation in the lattice of Ba_8Ge_{43}. Model A corresponds to M/Ge substitution at a constant level of vacancies (three voids per formula as observed in binary $Ba_8Ge_{43}\square_3$).[6] In model A the variation of composition is described by formula $Ba_8M_xGe_{43-x}\square_3$. Model B suggests that M atoms at first enter the three empty lattice sites and only after completely filling these sites at $x=3$, atoms M start to substitute for germanium adhering to the formula $Ba_8M_{3+x}Ge_{43-x}$. Experimental data for M=Cd and Zn (Refs. 2 and 3) clearly show a behavior intermediate between these two models, i.e., (Cd and Zn) atoms fill vacancies and simultaneously substitute for Ge-atoms in the framework, while the incorporation of Pd and Pt atoms is close to model B. Figure 4 summarizes the temperature dependency (100–300 K) of thermal atomic displacement parameters (ADP's) obtained from refinement of x-ray single crystal intensities of $Ba_8Pt_{2.7}Ge_{41.7}\square_{1.6}$. A large anisotropy of electron densities is obvious in two cases: (i) Ba2 atoms in the 6c site and (ii) Ge atoms in 24k site (Ge3). The electron density of Ba2 atoms in the big tetrakaidecahedral cages of the Ge framework adopts a form of flattened rotational ellipsoid with a volume about 20 times higher than that for Ba1 atoms in the smaller pentagondodecahedral cages of the clathrate lattice. The shape of the 24k site (Ge3) electron density adopts an ellipsoid elongated along the direction of the Ge1-Ge3 bonds. This 24k site was found to be split into two 24k sites (Ge31

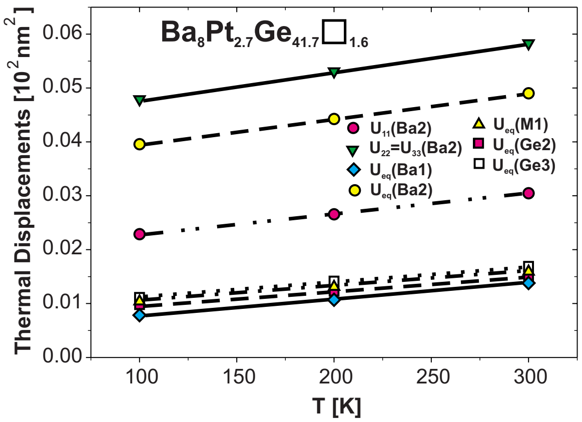

FIG. 4. (Color online) Temperature displacement parameters of $Ba_8Pt_{2.7}Ge_{41.7}\square_{1.6}$ vs temperature. M1 denotes a random mixture of [0.442 Pt+0.302(5) Ge+0.256 vacancy] as shown in Fig. 2.

and Ge32) for $Ba_8M_xGe_{46-x-y}\square_y$ (M=Pd,Zn,Cd) (Refs. 2–4) and for binary $Ba_8Ge_{43}\square_3$.[6] The split correlates well with the number of vacancies in the 6d site and the electron density centered at 24k adopts a regular shape for compositions that contain no vacancies in the 6d site. Also for our crystal with composition $Ba_8Pt_{2.7}Ge_{41.7}\square_{1.6}$ refinement using split atom positions (occGe31+occGe32=1) decreases the reliability factor from about 3.4% to 2.5% and reduces the residual electron density from 3.5 to less than 1.9 $e^-/\text{Å}^3$ yielding a featureless difference-Fourier map $F_{obs}-F_{calc}$.

The small difference among the atomic radii of Pt and Ge is reflected in an insignificant variation of the crystallographic parameters with Pt content (lattice parameter, atomic coordinates, and site occupancy). Distances monotonically increase following the trend defined by the unit cell dimensions (Fig. 1). As generally observed in clathrates,[2–4] the ADP parameters for Ba2 atoms in the 6c site show a significant anisotropy in contrast to Ba1 atoms, which behave normal with respect to the framework atoms (see Fig. 4). Such a behavior was first noticed by Reny *et al.* in Ba_8Si_{46}.[14] If the $Ba_8Pt_{2.7}Ge_{41.7}\square_{1.6}$ crystal is considered as a simple Debye solid with Ba2 atoms behaving like Einstein oscillators, the thermal displacements and the Einstein temperatures $\Theta_{E,ii}$ are related by

$$U_{ii} = \frac{\hbar^2}{2m_{\mathrm{Ba}}k_B\theta_{E,ii}} \coth\left(\frac{\theta_{E,ii}}{2T}\right), \tag{1}$$

where m_{Ba} is the atomic mass of Ba. From the linear slope $\Delta U_{ii}/\Delta T$ in Fig. 4 the force constants K_{ii}[gs^{-1}], the frequency of vibrations ν_{ii}[10^{12} s^{-1}], and hence the Einstein temperatures $\theta_{E,ii}$ [K] can be extracted. From symmetry constraints U_{11} for Ba2 is different from $U_{22}=U_{33}$ yielding $\theta_{E,11}$=96 K and $\theta_{E,33}$=82 K in line with the flat rotational ellipsoid of Ba2 atoms squeezed between the two hexagons of the framework tetrakaidecahedron. It is interesting to note that Ba1 atoms (spherical by symmetry) do not show a thermal displacement factor enhanced over the general ADP values for framework atoms. Thus, in contrast to Ba2, no special rattling effect can be seen for Ba1 atoms.

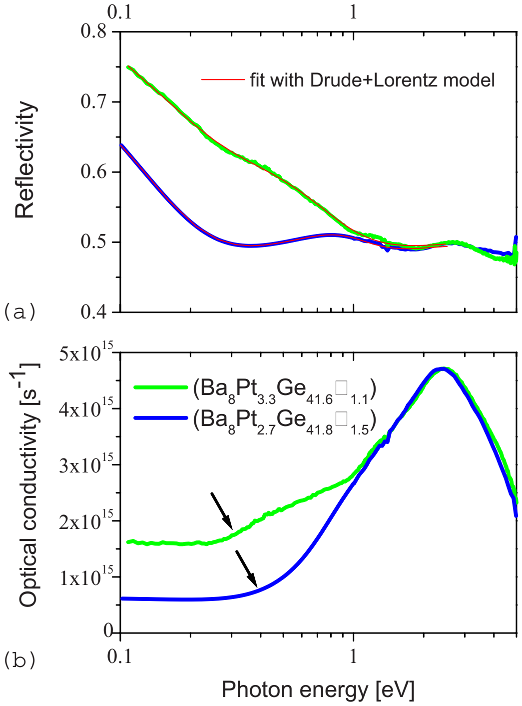

FIG. 5. (Color online) (a) Energy dependent reflectivity of $Ba_8Pt_xGe_{46-x-y}\square_y$ for x=2.7 and 3.3 measured at room temperature. The thin solid lines are least-squares fits. (b) Optical conductivity of $Ba_8Pt_xGe_{46-x-y}\square_y$ for x=2.7 and 3.3 as obtained by spectroscopic ellipsometry and KK analysis at room temperature.

C. Physical properties

Corresponding to the substitution of Ge/Pt and the accompanying change of the vacancy density $\square_y$ distinct changes of carrier concentration and thus of transport quantities such as resistivity and thermopower are expected in $Ba_8Pt_xGe_{46-x-y}\square_y$.

1. Optical measurements

The reflectance and the optical conductivity for the $Pt_{2.7}$ and the $Pt_{3.3}$ compounds are shown in Fig. 5.

Since ellipsometric spectroscopy is less affected by signal losses due to residual roughness, nonplanarity, and porosity of the surface, the reflectance as calculated by ellipsometric data is slightly larger than the one measured; hence the reflectance results have been shifted to match ellipsometry data. In this way one obtains a wide spectrum allowing us to perform Kramers-Kronig analyses to obtain both the real and imaginary parts of the dielectric function and optical conductivity over the whole spectrum. As a cross-check, the results of Kramers-Kronig coincide with the ellipsometric values obtained in the spectral region where they have been measured.

The spectra for $Ba_8Pt_{2.7}Ge_{41.8}\square_{1.5}$ and $Ba_8Pt_{3.3}Ge_{41.6}\square_{1.1}$ are very similar, particularly at the highest energies. A remarkable difference in the reflectivity is observed just in the infrared region where a metallic behavior occurs. Such a difference is reflected also in the optical conductivity spectrum where larger conductivity values are measured for $Ba_8Pt_{2.7}Ge_{41.8}\square_{1.5}$ than for $Ba_8Pt_{3.3}Ge_{41.6}\square_{1.1}$. Besides, con-

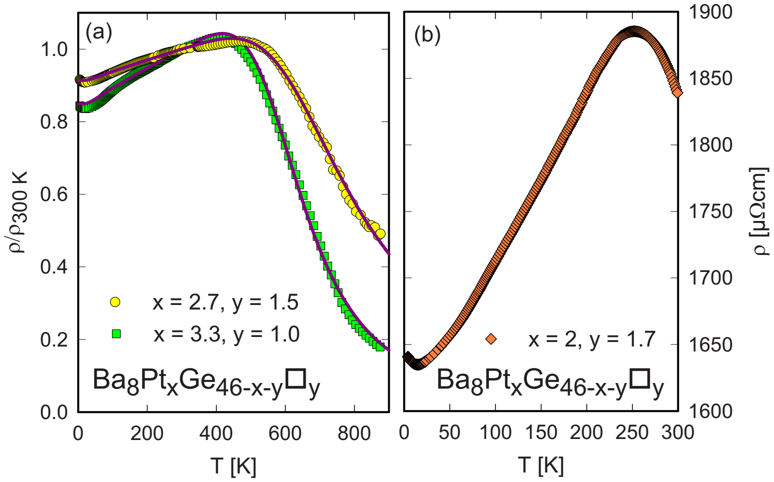

FIG. 6. (Color online) Temperature dependent resistivity ρ of various concentrations of $Ba_8Pt_xGe_{46-x-y}\square_y$, plotted in a normalized representation (a) and on an absolute scale (b). The solid lines are least-squares fits as explained in the text.

ductivity data exhibit a change of slope and an increase of intensity around 0.3–0.4 eV (indicated by arrows in the figure); this is direct evidence of a gap, i.e., the absorption edge of interband transitions (corresponding to roughly 3500–5000 K).

For a quantitative estimate of free carrier behavior, a fit has been performed on the reflectivity data within the spectral range 0.1–2 eV, with a model including a Drude term to account for the metallic behavior and two Lorentz oscillators to model interband transitions. The model parameters have furthermore been used to reproduce separately the real and imaginary parts of the dielectric function. The plasma frequencies thus obtained are $\omega_p^2=1.8$ eV and $\omega_p^2=3.1$ eV for $Ba_8Pt_{2.7}Ge_{41.8}\square_{1.5}$ and $Ba_8Pt_{3.3}Ge_{41.6}\square_{1.1}$, respectively, corresponding to effective carrier densities of $n=1.3\times10^{21}$ cm^{-3} and $n=2.2\times10^{21}$ cm^{-3}. The estimated resistivities at zero frequency [as deduced also from Fig. 5(b)] are 1400 and 600 $\mu\Omega$ cm for $Ba_8Pt_{2.7}Ge_{41.8}\square_{1.5}$ and $Ba_8Pt_{3.3}Ge_{41.6}\square_{1.1}$, respectively, in line with the increasing charge carrier density.

2. Temperature dependent electronic and thermal transports

Results of resistivity measurements taken in a wide temperature range for various concentrations of $Ba_8Pt_xGe_{46-x-y}\square_y$ are displayed in Figs. 6(a) and 6(b). Due to mechanical problems in handling the samples, absolute resistivity data are given only in the case of the Pt_2 system [Fig. 6(b)], where the $\rho(T)$ data obtained are quite large, referring to a reduced charge carrier density. Resistivity values normalized to room temperature are displayed for the $Pt_{2.7}$ and $Pt_{3.3}$ compounds. According to the optical data, resistivity at room temperature is expected to decrease owing to the rising charge carrier density. The specific structures of $\rho(T)$ indicate that all the materials investigated are, in fact, very near to a semiconducting state. The overall behavior resembles both metallic- and activationlike behaviors, as reflected from positive and negative slopes in $\rho(T)$. In order to account for such distinct features, we have developed a model (see Ref. 15) combining the description of simple metals via the Bloch-Grüneisen law with a temperature dependent charge carrier density. The most relevant assumptions are an electronic density of states (DOS) represented by a rectangular band with a narrow band of unoccupied states right at the Fermi energy E_F sequenced by a gap of width Δ. The charge carrier density is then calculated via standard statistics considering the Fermi-Dirac distribution function. Details have been reported by Melnychenko-Koblyuk *et al.*[2] and by Berger.[15] Least-squares fits according to this procedure are shown in Fig. 6 as solid lines. The principal parameter is the gap width Δ, about 3900 K (=0.33 eV) for $x=2.7$ to 4100 K (=0.35 eV) for $x=3.3$, well in agreement with the aforementioned optical data. Although the applied model is quite simple, it fairly well describes the temperature dependent resistivity throughout the series $Ba_8Pt_xGe_{46-x-y}\square_y$. The metallic behavior derives from scattering of conduction electrons into unoccupied sites in reciprocal space just above the Fermi energy. Once this region of the DOS becomes occupied, electrons have to be promoted across the gap, originating in semiconducting features. A distinct exponential behavior is not observed because of the proximity to the metallic state.

The temperature dependent thermal conductivity, λ, of $Ba_8Pt_{2.7}Ge_{41.8}\square_{1.5}$ and $Ba_8Pt_{3.3}Ge_{41.6}\square_{1.1}$ has been measured from 4 K to room temperature. Based on the Wiedemann-Franz law, the data observed were separated into the lattice (λ_{ph}) and the electronic contribution (λ_e), with $\lambda=\lambda_e+\lambda_{ph}$. Results are shown in Fig. 7 for both λ_e and λ_{ph}. The overall thermal conductivity values are rather small, expectable for cage forming compounds which are filled by loosely bound electropositive elements. Due to the large electrical resistivity of both clathrates, $\lambda_e(T)$ is small, and near to room temperature stays below 25% of λ_{ph}. No low temperature maximum in $\lambda_{ph}(T)$ is observed in both cases, in contrast to Zn-, Cd-, and Pd-rich compounds $Ba_8\{Zn,Cd,Pd\}_xGe_{46-x-y}\square_y$. Comparing the absolute $\lambda(T)$ values of $Ba_8M_xGe_{46-x-y}\square_y$ with M=Zn, Pd, Cd, and Pt shows an overall decrease for the sequence Zn, Pd, Cd, and Pt,[2–4] as a consequence of the growing atomic masses involved. It is interesting to note that none of the samples investigated is characterized by a dip in $\lambda(T)$ at lower temperatures, attributed to resonance scattering. This mechanism is expected to have a significant impact on thermal transport and is considered responsible for the glasslike behavior in some cage forming compounds. An ar-

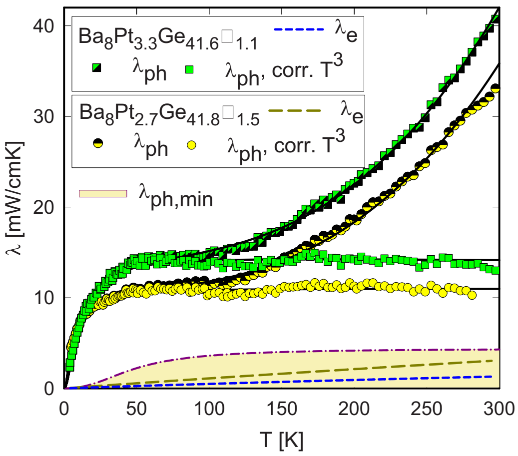

FIG. 7. (Color online) Lattice (λ_{ph}, filled and semifilled symbols) and electronic (λ_e, short- and long-dashed lines) thermal conductivities of $Ba_8Pt_{2.7}Ge_{41.8}\square_{1.5}$ and $Ba_8Pt_{3.3}Ge_{41.6}\square_{1.1}$. The data corresponding to the filled symbols are derived from those with semifilled symbols by subtracting a radiation-loss term proportional to T^3. The solid lines are least-squares fits according to Eq. (2). The dashed dotted line corresponds to the upper border of the theoretical lower limit of the lattice thermal conductivity.

chetypal example for the latter is $Eu_8Ga_{16}Ge_{30}$.[16]

A quantitative description of $\lambda(T)$ is possible in terms of Callaway and von Baeyer's theory[17] of lattice thermal conductivity, which follows from the basic thermodynamic expression $\lambda=(1/3)C_V v l$, where C_V is the heat capacity of the system, v the particle velocity, and l the mean free path. Hence,

$$\lambda_{ph} = \frac{k_B}{2\pi^2 v_s}\left(\frac{k_B}{\hbar}\right)^3 T^3 \int_0^{\theta_D/T} \frac{\tau_c x^4 e^x}{(e^x-1)^2}dx, \qquad (2)$$

with the velocity of sound $v_s=\frac{k_B\theta_D}{\hbar(6\pi^2 n)^{1/3}}$ and $x=\hbar\omega/k_BT$, where n is the number of atoms per unit volume and ω the phonon frequency. τ_c^{-1} is the sum of the reciprocal relaxation times for point defect scattering, τ_D^{-1}, Umklapp processes, τ_U^{-1}, boundary scattering, τ_B^{-1}, and scattering of phonons by electrons, τ_E^{-1}, i.e.,

$$\tau_c^{-1} = \tau_D^{-1} + \tau_U^{-1} + \tau_B^{-1} + \tau_E^{-1}. \qquad (3)$$

Equation (3) does not contain terms for resonance scattering, since they seem to be of minor importance in both compounds studied. In order to get rid of radiation losses, proprietary to the steady state heat flow method used, a T^3 term was added to Eq. (2) for the analysis.

The initial rise of λ_{ph} may be referred to boundary and point defect scattering; it becomes large when both quantities are small. Note that defects comprise also vacancies. In case of substantial Umklapp scattering processes, λ_{ph} would exhibit an exponential drop; in combination with τ_B and τ_D a maximum in $\lambda_{ph}(T)$ is then formed. The latter depends also weakly on the Debye temperature but occurs in general well below $\theta_D/10$. Additionally, an increase of θ_D slightly reduces overall λ_{ph} values. Enhanced scattering of phonons on electrons also efficiently reduces the lattice thermal conductivity.

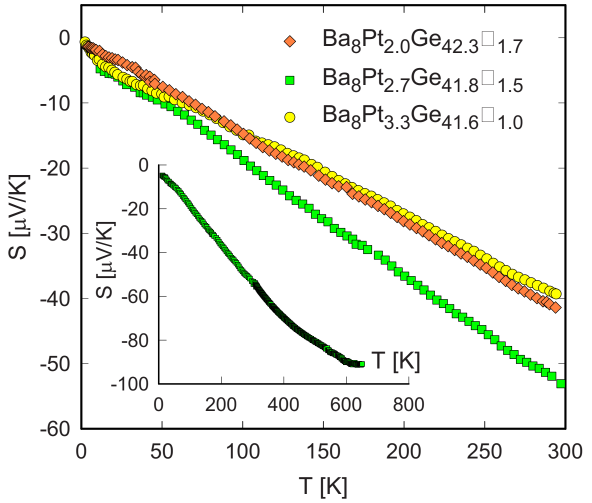

FIG. 8. (Color online) Temperature dependent thermopower $S(T)$ for various concentrations of $Ba_8Pt_xGe_{46-x-y}\square_y$; $x=2.0$, $x=2.7$, and $x=3.3$. The sample with $x=3.3$ was measured in an extended temperature range.

Least-squares fits according to Eq. (2) are shown in Fig. 7 as solid lines, revealing fine agreement with the data observed. Comparing the set of fit parameters indicates that the relaxation time referring to point defect scattering, i.e., $\tau_D^{-1}=Dx^4T^4$, with the material dependent parameter D decreases by more than a factor of 2 when proceeding from the sample with $x=2.7$ to the sample $x=3.3$. This result, which should be used only in a qualitative manner, reveals that, although the disorder due to the Ge/Pt substitution rises, the overall disorder of the crystal decreases much stronger due to the reduction of the vacancy content provoked by the growing Pt content (compare Fig. 3).

An approximation according to Cahill and Pohl[18] allows us to estimate the theoretical lower limit of the lattice thermal conductivity, which primarily is defined by the number of atoms per unit volume and by the Debye temperature. Taking $N=4.26\times10^{28}\ \mathrm{m}^{-3}$ and $\theta_D=230$ K [as derived from the least-squares fit according to Eq. (2)] for $Ba_8Pt_{3.3}Ge_{41.6}\square_{1.1}$ reveals $\lambda_{min}(300\ \mathrm{K})=4.3$ mW/cm K. Results below room temperature are shown in Fig. 7 as hatched area.

Results regarding the temperature dependent thermopower, S, are plotted in Fig. 8 for various concentrations of $Ba_8Pt_xGe_{46-x-y}\square_y$. $S(T)$ is negative in the entire range of temperatures investigated indicating electrons as the dominant charge carriers. For all three compositions an almost linear $S(T)$ dependence is observed reaching about $\approx 90\ \mu$V/K at 600 K for $Ba_8Pt_{3.3}Ge_{41.6}\square_{1.1}$. The almost linear temperature dependence of $S(T)$ rules out significant correlations among charge carriers; then the slope of $S(T)$ depends primarily on the charge carrier density n. As demonstrated, e.g., in Ref. 3, the diffusion part of the thermopower can simply be represented by

$$S_d = \frac{\pi^2 k_B^2 2m_e}{e\hbar^2(3n\pi^2)^{2/3}}T, \qquad (4)$$

where m_e is the mass of the carriers and e is the respective charge. Approaching the data of Fig. 8 by a linear dependence for $T < 300$ K allows calculating the charge carrier density [Eq. (4)], which for the $Pt_{2.7}$ compound amounts to $n = 1.25 \times 10^{21}$ cm^{-3} and for $Pt_{3.3}$ is $n = 2.02 \times 10^{21}$ cm^{-3}. These figures are in perfect agreement with the results of the aforementioned optical reflectivity data. The analysis for $Pt_{2.0}$ yields $n = 1.8 \times 10^{21}$ cm^{-3}. A further justification for such an estimation of n from thermopower data was previously corroborated by Hall-effect measurements on $Ba_8(Ge,Pd)_{46}$.[4]

IV. SUMMARY

Starting from binary $Ba_8Ge_{43}\square_3$ a series of clathrates was synthesized forming a solid solution $Ba_8Pt_xGe_{46-x-y}\square_y$, with a solubility limit of 3.5 Pt atoms/f.u. at 800 °C. Throughout the homogeneity region cubic primitive symmetry consistent with the clathrate type I has been confirmed. Phase relations were derived at subsolidus temperatures as well as at 800 °C.

Physical properties, such as charge carrier density and transport quantities, were found to be heavily influenced by the Ge/Pt substitution in the clathrate framework. From electrical resistivity data the series can be classified to be located close to a semiconducting regime with a gap in the electronic density of states of a few thousand K. The gradual change observed is a function of the combined effect of Ge/Pt substitution and the reduction of vacancies. Thermal conductivity data are modeled in terms of Callaway and von Baeyer's theory of heat carrying phonons. The efficiency of scattering vacancies is evidenced from the thermal conductivity study.

Thermopower indicates that the majority charge carriers are electrons, with a slight variation of the charge carrier density (being in the order of $n \approx 10^{21}$ cm^{-3}) as a function of the Pt content. Additionally, $S(T)$ basically defines the figure of merit $Z \cdot T = S^2 T / (\rho \cdot \lambda)$, which represents the thermoelectric performance of a certain material. Using the compound with the highest Seebeck coefficient, i.e., $x = 2.7$ reveals $ZT \approx 0.15$ at 600 K.

ACKNOWLEDGMENTS

The research reported herein was sponsored by the Austrian FWF projects P19165 and P16778-No2 and supported by the EU-network of excellence CMA (*Complex Metallic Alloys*, Contract No. NMP3-CT-2005-500140).

---

[1] A. Saramat, G. Svensson, A. E. C. Palmqvist, C. Stiewe, E. Mueller, D. Platzek, S. G. K. Williams, D. M. Rowe, J. D. Bryan, and G. D. Stucky, J. Appl. Phys. **99**, 023708 (2007).

[2] N. Melnychenko-Koblyuk, A. Grytsiv, S. Berger, H. Kaldarar, H. Michor, F. Röhrbacher, E. Royanian, E. Bauer, P. Rogl, H. Schmid, and G. Giester, J. Phys.: Condens. Matter **19**, 046203 (2007).

[3] N. Melnychenko-Koblyuk, A. Grytsiv, L. Fornasari, H. Kaldarar, H. Michor, F. Röhrbacher, M. Koza, E. Royanian, E. Bauer, P. Rogl, M. Rotter, H. Schmid, F. Marabelli, A. Devishvili, M. Doerr, and G. Giester, J. Phys.: Condens. Matter **19**, 216223 (2007).

[4] N. Melnychenko-Koblyuk, A. Grytsiv, P. Rogl, M. Rotter, E. Bauer, G. Durand, H. Kaldarar, R. Lackner, H. Michor, E. Royanian, M. Koza, and G. Giester, Phys. Rev. B **76**, 144118 (2007).

[5] W. Carrillo-Cabrera, J. Curda, K. Petters, M. Baenitz, Y. Grin, and H. G. von Schnering, Z. Kristallogr. - New Cryst. Struct. **215**, 321 (2000).

[6] W. Carrillo-Cabrera, S. Budnyk, Y. Prots, and Y. Grin, Z. Anorg. Allg. Chem. **630**, 7226 (2004).

[7] G. Cordier and P. Woll, J. Less-Common Met. **169**, 291 (1991).

[8] W. Carrillo-Cabrera, H. Borrmann, S. Paschen, M. Baenitz, F. Steglich, and Y. Grin, J. Solid State Chem. **178**, 715 (2005).

[9] R. Demchyna, Yu. Prots, W. Schnelle, U. Burkhardt, and U. Schwarz, Z. Kristallogr. - New Cryst. Struct. **221**, 109 (2006).

[10] E. Bauer, A. Grytsiv, Xing-Qiu Chen, N. Melnychenko-Koblyuk, G. Hilscher, H. Kaldarar, H. Michor, E. Royanian, G. Giester, M. Rotter, R. Podloucky, and P. Rogl, Phys. Rev. Lett. **99**, 217001 (2007).

[11] T. B. Massalski, *Binary Alloy Phase Diagrams*, 2nd ed. (ASM International, Metals Park, OH, 1990).

[12] E. Parthé, L. Gelato, B. Chabot, M. Penzo, K. Cenzual, and R. Gladyshevskii, *TYPIX—Standardized Data and Crystal Chemical Characterization of Inorganic Structure Types* (Springer-Verlag, Berlin, 1994).

[13] H. Fukuoka, K. Iwai, S. Yamanaka, H. Abe, K. Yoza, and L. Häming, J. Solid State Chem. **151**, 117 (2000).

[14] E. Reny, A. San-Miguel, Y. Guyot, B. Masenelli, P. Melinon, L. Saviot, S. Yamanaka, B. Champagnon, C. Cros, M. Pouchard, M. Borowski, and A. J. Dianoux, Phys. Rev. B **66**, 014532 (2002).

[15] St. Berger, Ph.D thesis, Vienna University of Technology, 2003.

[16] J. L. Cohn, G. S. Nolas, V. Fessatidis, T. H. Metcalf, and G. A. Slack, Phys. Rev. Lett. **82**, 779 (1999).

[17] J. Callaway and H. C. von Baeyer, Phys. Rev. **120**, 1149 (1960).

[18] D. Cahill and R. Pohl, Solid State Commun. **70**, 927 (1989).